RSC Advances

PAPER

Cite this: *RSC Adv.*, 2014, **4**, 58930

Plasmon-mediated, highly enhanced photocatalytic degradation of industrial textile dyes using hybrid ZnO@Ag core–shell nanorods†

V. P. Dinesh,[a] P. Biji,*[a] Anuradha Ashok,[a] S. K. Dhara,[b] M. Kamruddin,[b] A. K. Tyagi[b] and Baldev Raj[a]

Hybrid ZnO@Ag core–shell heterojunction nanorods were synthesized using a novel, facile two-step process based on hydrothermal and seed mediated growth techniques. The material was characterized by UV-visible spectroscopy, Fourier transform-infrared spectroscopy (FT-IR), room temperature photoluminescence spectroscopy (RTPL), Raman spectroscopy, thermogravimetric analysis (TGA), X-ray diffraction (XRD), high resolution transmission electron microscopy (HRTEM) and X-ray photoelectron spectroscopy (XPS). The hybrid ZnO@Ag core–shell nanorods were comprised of one-dimensional (1D) ZnO nanorods serving as a core material, over which surface-doped Ag nanoclusters (~2.5 nm) were anchored as a heterogeneous shell. The presence of oxygen vacancies and Zn interstitials were confirmed by RTPL and Raman spectroscopic analysis. The photocatalytic activity of the hybrid ZnO@Ag core–shell nanorods was studied in comparison to bare ZnO nanorods using standard R6G dye and industrial textile dyes such as Congo red and Amido black 10B under UV and visible light (solar) irradiations. Moreover, the material was tested for real time industrial textile effluents under ambient conditions and was found to be highly efficient. The enhanced photocatalytic property observed for ZnO@Ag hybrid core–shell nanorods is attributed to a phenomenal increase in oxygen related defects in the core that generate photo-induced charge carriers and the presence of plasmonic Ag nanoclusters in the shell, which act as a sink for the photo-induced charge carriers.

Received 28th August 2014
Accepted 20th October 2014

DOI: 10.1039/c4ra09405k

www.rsc.org/advances

Introduction

The residual dyes from textile and various industries are considered to be the major constituents of organic pollutants when introduced to natural water resources causing severe environmental pollution. About 2–20% of the dyes used in a dyeing process are released as textile effluents.[1] These colored organic dyes provoke serious environmental hazards by engendering water pollution and eutrophication to aquatic lives and can stimulate perilous products through chemical reactions.[2] Hence, the degradation of organic pollutants such as textile dyes has received considerable attention, leading to an environmental remedial process. There are numerous non-destructive physical processes used for the degradation of textile and industrial dyes. However, they just transfer the organic compounds into another phase causing secondary pollutants.[3] Similarly, biological and chemical methods are performed at the dawdling phase with high operating costs.[4] Current practices and technologies are inadequate; the need for eco-friendly and cost effective remedies has paved the way for the emergence of a new destructive technique, known as advanced oxidation processes (AOPs). In this process, very reactive species like hydroxyl radicals ($OH^{\bullet}$) oxidize a wide range of organic pollutants rapidly and randomly leading to the complete mineralization of organic dyes into CO_2. AOPs have been used by varied processes starting from Fenton, photo-Fenton catalytic reactions, UV-H_2O_2 processes, and TiO_2 mediated photocatalysis.[5] Among the various materials used for AOPs, semiconducting metal oxide materials are inexpensive, non toxic and possess high chemical stability. Metal oxide semiconductors (MOS) such as ZnO and TiO_2, having wide band gaps, have widely been used as photocatalysts owing to their high catalytic properties and environmental sustainability.[6,7] However, it is found that the photocatalytic efficiency of MOS is significantly affected due to the recombination (up to 90%) of photogenerated charge carriers,[8] whereas nanosized MOS (both 0D and 1D) have more advantage over their bulk due to their increased surface-to-volume ratio, size comparable to the Debye

[a]*Nanotech Research Facility, PSG Institute of Advanced Studies, Coimbatore-641004, India. E-mail: bijuja123@yahoo.co.in; Fax: +91-42-2257-3833; Tel: +91-422 4344000 ext. 4193*

[b]*Indira Gandhi Center for Atomic Research, Kalpakkam-603102, India. Fax: +91-44-27480081; Tel: +91-44-27480500 ext. 22507*

† Electronic supplementary information (ESI) available: FT-IR, TGA, FE-SEM studies and XRD of hybrid ZnO@Ag core–shell nanorods, XRD studies of ZnO nanorods, photocatalytic degradation profiles of R6G, Amido black 10B and Congo red using ZnO nanorods and pH dependent photocatalytic degradation of ZnO@Ag core–shell nanorods. See DOI: 10.1039/c4ra09405k

screening length, more active sites and reduced recombination process.[9] Though zero-dimensional (0D) TiO_2 and ZnO nanoparticles exhibit enhanced photocatalytic properties when compared to their bulk counterparts, retrieving these fine powdered photocatalysts from the photocatalytically treated water is very difficult, which affects the reutilization process.[10] Apart from this, the aggregation of 0D nanoparticles occurs in solution state, which drastically affects the efficiency by inhibiting the formation of hydroxyl radicals. To overcome these hindrances, 1D nanomaterials are the most suitable candidates, as they are highly stable against aggregation and are also easily recovered after photocatalysis. Apart from this, 1D nanostructure has a faster electron diffusion process than 0D particles due to the formation of a space charge layer, which acts as an energetic barrier in the recombination process.[11]

The photocatalytic efficiency of MOS can be further increased significantly by introducing metal/semiconductor hetero-junctions, since noble metals (Au, Ag and Pt) can act as reservoirs for photo-generated electrons; thereby supporting interfacial charge separation processes.[12,13] The synthesis of hybrid 1D semiconductors with heterojunctions is a challenging process and has been carried out using a number of chemical methods such as co-precipitation, chemical vapour deposition, hydrothermal deposition–precipitation.[14,15] However, some of the important issues still persist and are yet to be addressed during the formation of hybrid nanostructures. The uniform deposition of metal nanoparticles with a controlled size over the semiconductors is one of the key issues in research. TiO_2 based hybrid nanoparticles have been extensively used as photocatalysts while, the ZnO based hybrid nanostructures have not been much exploited. It is to be mentioned that ZnO can be tailor made into any nanostructure and dimensions as per our applications by adopting simple synthetic routes. Moreover, ZnO can also be used as a feasible alternative to TiO_2 with a wide band gap of 3.37 eV, very large exciton energy of 60 meV, and an electron affinity of 4.2 eV, making it a promising material for a variety of applications.[16] Among noble metal catalysts, Ag doped MOS has shown promising efficiency for varied applications because of its unique plasmonic properties and antimicrobial effects.[17] Recently, scientists have reported that Ag doped heterojunction nanoparticles show an enhanced photocatalysis with increased efficiency due to the photoinduced electron transfer process upon UV irradiation.[18] Therefore, for investigation, Ag was chosen to form heterojunctions on the surface of 1D ZnO nanorods forming ZnO@Ag core–shell nanorods. Though there are numerous approaches for the synthesis of Ag/ZnO based heterostructures using wet chemical and hydrothermal routes,[19] the major difficulty observed in these methods is that Ag nanoparticles tend to form aggregates rather than nanoclusters. The aggregation of Ag nanoparticles will directly affect the efficiency of photocatalysis and photoelectric properties because of the decreased contact between Ag and ZnO interfaces. As a result, the rational synthesis of ZnO@Ag core–shell nanorods with a specific 1D morphology and well-defined interface directly plays a significant role in the charge transport properties. Thus, it is essential to develop simple and efficient methods for the controlled deposition of Ag nanoclusters onto the surface of 1D MOS. The deposition of Ag nanoclusters onto 1D SMOs plays an important role in charge distribution and consequently influences the optical and photocatalytic properties. Herein, we report a novel, facile two-step process for the synthesis of hybrid ZnO@Ag core–shell heterojunction nanorods at room temperature with an Ag nanoclusters surface decorated over the ZnO nanorods. Though several precipitation and reduction methods were reported for the synthesis of core–shell heterojunctions, we have adopted a simple seed mediated growth method using triethylamine (TEA) as the reducing agent. The slow reduction process using a weak reducing agent, TEA was found to be highly efficient in controlling the nanocluster formation during seed mediated growth, compared to previous reports. In addition, the well-defined interfaces between ZnO and Ag, and a favoured crystallographic relationship between the metal nanoparticles and MOS have been identified. According to many reports, some external factors like heat treatment are required to enhance the photocatalysis process.[20,21] However, for the method reported in this work, no such treatment is required. Hybrid ZnO@Ag core–shell nanorods produced using this synthetic strategy were found to exhibit excellent photocatalytic properties towards the degradation of R6G, Congo red and Amino black dyes owing to the plasmonic effects of Ag nanoclusters on the ZnO nanorod surface. Interestingly, the material showed a good degradation efficiency for real time industrial textile effluents also, under both UV and solar irradiations. The active role of the plasmonic Ag nanoclusters on the ZnO nanorods during photocatalysis and the probable mechanism is discussed and proposed. The synthetic strategy revealed in this study followed by its photocatalytic applications paves a way for a realistic solution needed in the textile industry.

Experimental section

Materials and methods

Zinc chloride (98%, Merck), potassium hydroxide (98%, Merck), silver nitrate (99.9%, Merck), cetyl trimethylammonium bromide (CTAB) (99%, Merck), ethanol (99%, Merck), triethylamine (TEA) (99% Merck) and 3-aminopropyl-trimethoxysilane (APTMS) (99%, Aldrich) were taken as precursors. All chemicals were used as received without any further purification. Ultrapure water with a resistivity of 18.2 MΩ cm was used (Millipore Milli-Q system) for the synthesis.

Synthesis of ZnO nanorods

The ZnO nanorods used in this study were prepared according to a previously reported procedure.[22] In brief, 10 mL of 2 mM KOH solution was added dropwise into 20 mL of 1 mM $ZnCl_2$ solution and stirred vigorously. 5 mL of 0.5 mM CTAB solution was added to the stirred solution, and white floccules appeared immediately, indicating the formation of zinc hydroxide. After 3 hours of continued stirring, the solution was transferred into a Teflon-lined stainless steel autoclave and filled by distilled water up to 80% volume. Hydrothermal treatments were carried out at 120 °C

for 5 h. After this process, the autoclave was allowed to cool down naturally, and white precipitates of ZnO nanorods were separated *via* centrifugation and washed thoroughly using distilled water and ethanol to remove impurities. Finally, the ZnO nanorods were dried at 80 °C in a hot air oven for 8 h.

Synthesis of hybrid ZnO@Ag core–shell nanorods

In order to functionalize the ZnO nanorods, 2 mg of the ZnO nanorods were weighed and dispersed in 10 mL of 1 M ethanol. 50 μL of 1 M 3-aminopropyl-trimethoxysilane (APTMS) was added to the dispersion and continuously stirred for 12 h. After completion of the functionalization reaction, the precipitate was separated and washed several times using distilled water and ethanol, and further dried at 60 °C. 10 mL of 7.5 M triethylamine (TEA) solution was taken in a round bottom flask, and 2 mg of APTMS functionalized ZnO nanorods were added and stirred for 30 minutes. 2 mL of 0.6 M of $AgNO_3$ solution was added dropwise to the mixture. A dark brown precipitate was formed immediately after the addition, indicating the formation of ZnO@Ag core–shell nanorods. 100 mL of distilled water was added to the dark brown precipitate, and the solution was left undisturbed for 5 hours for seed growth. The precipitate was separated and purified carefully using distilled water and ethanol several times and finally vacuum filtered to remove impurities. Further, the materials were air dried overnight at 80 °C. The purified hybrid ZnO@Ag core–shell nanorods were further used for the photocatalytic degradation of R6G and industrial textile dyes.

Characterization techniques

The purified ZnO@Ag nanorods were well characterized spectroscopically and microscopically. UV-vis absorption spectra were acquired using a T90+UV-visible spectrophotometer (PG Instruments, UK). The FT-IR analysis was performed by a Nicolet Impact 400 FT-IR spectrophotometer using KBr pellets. Micro Raman and PL studies were conducted using a He–Cd laser as the excitation light source at 325 nm with 2400 g mm^{-1} gratings in the backscattering configuration of a spectrometer (inVia Renishaw, UK). Thermogravimetric analysis was completed using Perkin Elmer STA 600 instruments with a scanning rate of 10° min^{-1}. Powder XRD patterns were taken for all the calcined samples by a XRD power X-ray diffractometer (JSO-DEBYEFLEX 2002) using Cu Kα radiation of wavelength 1.54 nm with a scanning rate of 0.02° s^{-1} in the 2θ range of 10–70°. The structure and morphology of the hybrid core–shell nanomaterials were examined using high-resolution transmission electron microscopy (JEOL JEM-2010, Japan) and field emission scanning electron microscope (ZEISS SUPRA 55) in-built with an energy-dispersive X-ray spectrometer (Oxford Instruments, INCA, UK). X-ray photoelectron spectroscopy (Omicron Nanotechnology, Germany) was used to analyze the structural composition of the ZnO@Ag hybrid nanostructures.

Photocatalytic dye degradation studies

The photocatalytic properties of the hybrid ZnO@Ag core–shell nanorods were evaluated by observing the catalytic degradation of rhodamine 6G standard dye. The photocatalytic experiments were performed under atmospheric conditions. An aqueous solution of R6G dye was treated with hybrid ZnO@Ag core–shell nanorods immediately before the experiment and purged with nitrogen to remove any dissolved oxygen. The concentration of the catalyst in the reaction mixture was optimized as 25 mg L^{-1} against the dye concentration of 10 ppm. The catalyst suspension was mixed thoroughly using ultrasonication (15 min) to attain equilibrium adsorption on the catalyst surface. Photocatalysis was performed using UV radiation from a fluorescent Hg lamp (Philips TUV 4W: the strongest emission around $\lambda = 360$ nm). Under similar conditions, experiments were also carried using full spectrum solar simulator with a Abet 10500 Class A Solar Simulator fitted with a Xenon arc lamp (AM = 1.5 G). The photocatalytic degradation was monitored using UV-vis spectroscopy by measuring the absorption of R6G at 525 nm as a function of irradiation time. All the absorbance values were averaged out of three independent measurements. Similar experiments were conducted using industrial textile dyes such as Congo red and Amido black to establish the dye degradation efficiency using the ZnO@Ag core–shell nanorods. Industrial textile effluents used for real sample testing were collected from a textile industry located in Thirupur, India.

Results and discussion

Hybrid core–shell nanorods were prepared *via* a combination of hydrothermal method and *in situ* reduction method using bifunctional ligands. Hydrothermally synthesized ZnO nanorods were used as the core, which were further functionalized using APTMS ligands. The APTMS functionalized ZnO nanorods were then treated with $AgNO_3$ and *in situ* reduced using TEA, and a dark brown precipitate of hybrid ZnO@Ag core–shell nanorods was obtained. Fig. 1 represents the schematic representation of hybrid core–shell nanorods formation.

UV-visible absorbance spectra of the ZnO nanorods and ZnO@Ag hybrid nanorods are shown in Fig. 2a. The characteristic peak appearing at 370 nm corresponds to the ground excitonic peak of pure ZnO nanorods.[23] The absence of additional adsorption peaks in the UV-visible spectrum further confirms the purity of the ZnO nanorods. In hybrid ZnO@Ag core–shell nanorods, a red shifted peak at 373 nm was observed due to the strong interfacial electronic coupling between the ZnO and Ag atoms.[24] In the heterostructures, an electron transfer process occurs from ZnO and Ag owing to a divergence in the Fermi levels.[24] A sharp peak centered at 270 nm is observed for the hybrid ZnO@Ag core–shell nanorods, which reveals the presence of silver nanoclusters having diameters less than 5 nm.[25] Here, TEA was used to reduce the Ag^+ ions to form Ag^0, which is a weak reducing agent compared to sodium borohydride.[26] The *in situ* reduction of Ag^+ leads to the formation of Ag nanoclusters on the surface of ZnO nanorods. The Ag^0 atomic clusters thus formed create nucleation centers on the surface of APTMS functionalized ZnO nanorods for further growth as nanoclusters. The domination of Ag nanoclusters over Ag nanoparticles gives rise to an inconspicuous shoulder peak at 270 nm, decreasing its plasmon peak to 420 nm.

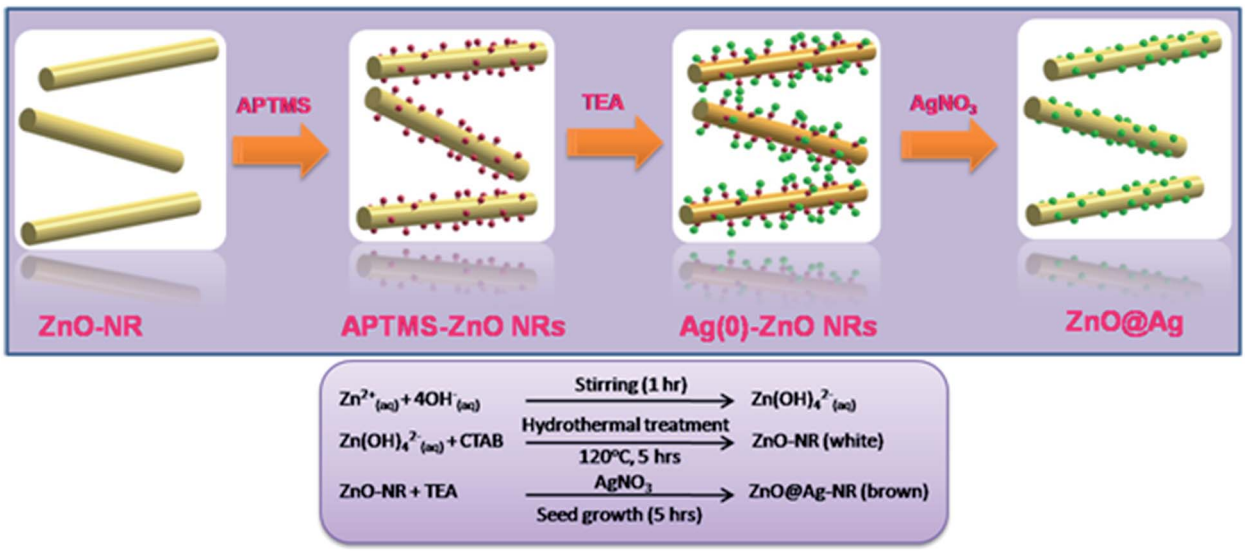

Fig. 1 Schematics of the synthetic process adopted for the growth of hybrid ZnO@Ag nanorods.

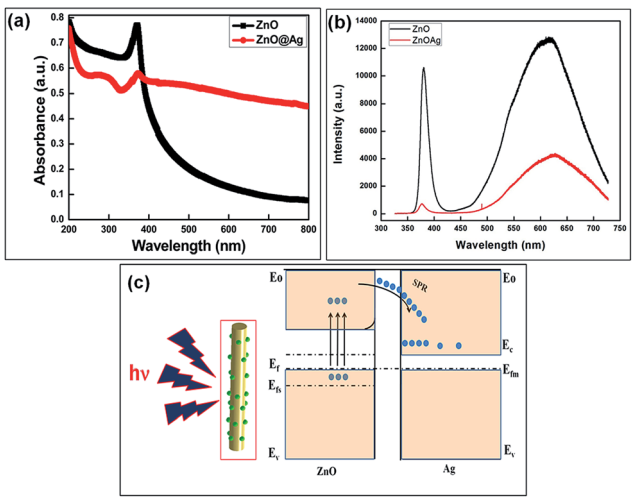

Fig. 2 (a) UV-visible spectra of ZnO nanorods and hybrid ZnO@Ag core–shell nanorods, (b) PL spectrum of ZnO nanorods and hybrid ZnO@Ag core–shell nanorods and (c) the energy band structure of hybrid ZnO@Ag core–shell nanorods.

Moreover, the exciton peak of ZnO at 373 nm dominates over the plasmon peak of Ag nanoparticles. This can be attributed to defects being utilized for Ag nanocluster growth over the ZnO nanorods.[27] A similar effect was observed in Au nanoclusters described in previous reports, where the surface plasmon absorbance decreases as a function of reduction in cluster size.[28] Thus, optical absorbance studies reveal the formation of Ag nanoclusters on the surface of ZnO nanorods, which was further confirmed from the HR-TEM analysis. Photoluminescence studies offer an insight into the optical and photochemical properties of the hybrid ZnO@Ag core–shell nanorods. The PL spectra revealed structural defects such as oxygen vacancies and zinc interstitials, as well as the charge distribution and Fermi level equilibrium in the ZnO@Ag heterostructures. The room temperature PL spectra (excitation at 325 nm) for ZnO and hybrid ZnO@Ag nanorods are depicted in Fig. 2b. A strong excitation peak shows a UV emission band centered at 380 nm corresponding to the near band edge emission of ZnO nanorods due to excitonic recombination through an exciton–exciton collision process and reflects the high crystalline nature of the ZnO nanorods.[29] The high intensity peaks observed at the yellow-orange region and green emission regions (Fig. 2b) are due to the presence of oxygen related defects and interstitials present in the ZnO nanorods.[30,31] The PL intensity of hybrid ZnO@Ag core–shell nanorods appear to be lower when compared to ZnO nanorods. This can be attributed to the formation of Ag nanoclusters over ZnO nanorods, which accept electrons and lead to the increased charge separation effects for photo-induced electrons–holes pairs. As the Ag nanoclusters start growing over the ZnO nanorods, the decline of crystal defects occurs primarily leading to the relaxed nature of charge carriers *via* surface related traps, and thereby quenching the emission peak of ZnO. This process influences the charge carrier dynamics of the hybrid materials.[31,32] The decrease in emission intensity is in accordance with the Stern–Volmer quenching effect reported in the literature.[33] Variation of $V_O^{\cdot\cdot}$ defect density on the surface of ZnO nanorods is related to the high surface-to-volume ratio and the interfaces between Ag nanoclusters and ZnO nanorods.[20] Upon irradiation of incident light with a wavelength larger than the particle size, a high-density electron cloud of noble metal nanoclusters forms and tends to oscillate. In the hybrid materials, electrons accumulate at the metal–semiconductor junctions leading to upward band bending for ZnO, and thus favoring the straightforward transfer of an electron from ZnO to Ag nanoclusters, which prevents the charge carrier recombination process,[34] as depicted in Fig. 2c. From the PL studies, Ag nanoclusters on the ZnO surface block both direct trap related charge carrier recombination pathways by extracting electrons from the photoinduced ZnO.[18] Thus, a majority of the extracted

electrons are utilized for the catalytic degradation process leading to enhanced photocatalytic activity.

Morphological and structural analysis of the core–shell ZnO@Ag nanorods were further carried out using FE-SEM, X-ray diffraction studies and Raman spectral analysis. FE-SEM studies of the hybrid core–shell nanorods showed the monodispersed nanorods, and EDS showed the loading percentage of Ag onto ZnO nanorods of 6.90% (see Fig. S1, ESI†). XRD studies of the ZnO nanorods showed their characteristic peaks with a hexagonal wurtzite structure with a space group of $P6_3mc$. XRD data of the hybrid ZnO@Ag core–shell nanorods reveal peaks corresponding to Ag along with those of ZnO, confirming the formation of hybrid structures (see Fig. S2 and Table S1, ESI†). Raman spectroscopy is another powerful technique used to infer about the optical phonon modes, phase purity and vibrational properties of the ZnO nanorods and ZnO@Ag hybrid core–shell nanorods. ZnO nanorods show two asymmetric longitudinal optical multi-phonon peaks at 579 and 1150 cm^{-1}, whereas hybrid ZnO@Ag core–shell nanorods shows red shift for LO phonon modes with an appreciable peak broadening effect due to the growth of Ag nanoclusters onto the ZnO nanorods (see Fig. S3, ESI†). FE-SEM and TEM images of the bare ZnO nanorods synthesised by the hydrothermal method are shown in Fig. 4a and b. As evident from the microscopic

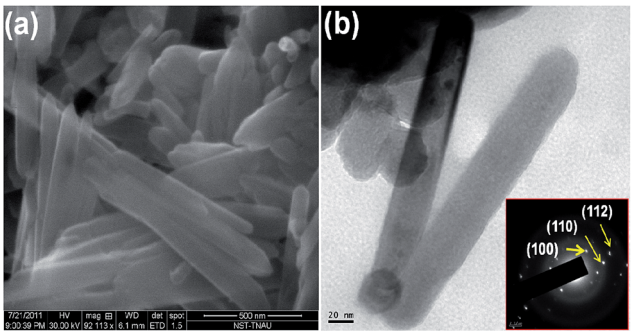

Fig. 4 (a) FE-SEM image and (b) TEM image of bare ZnO nanorods (inset shows the SAD pattern of ZnO).

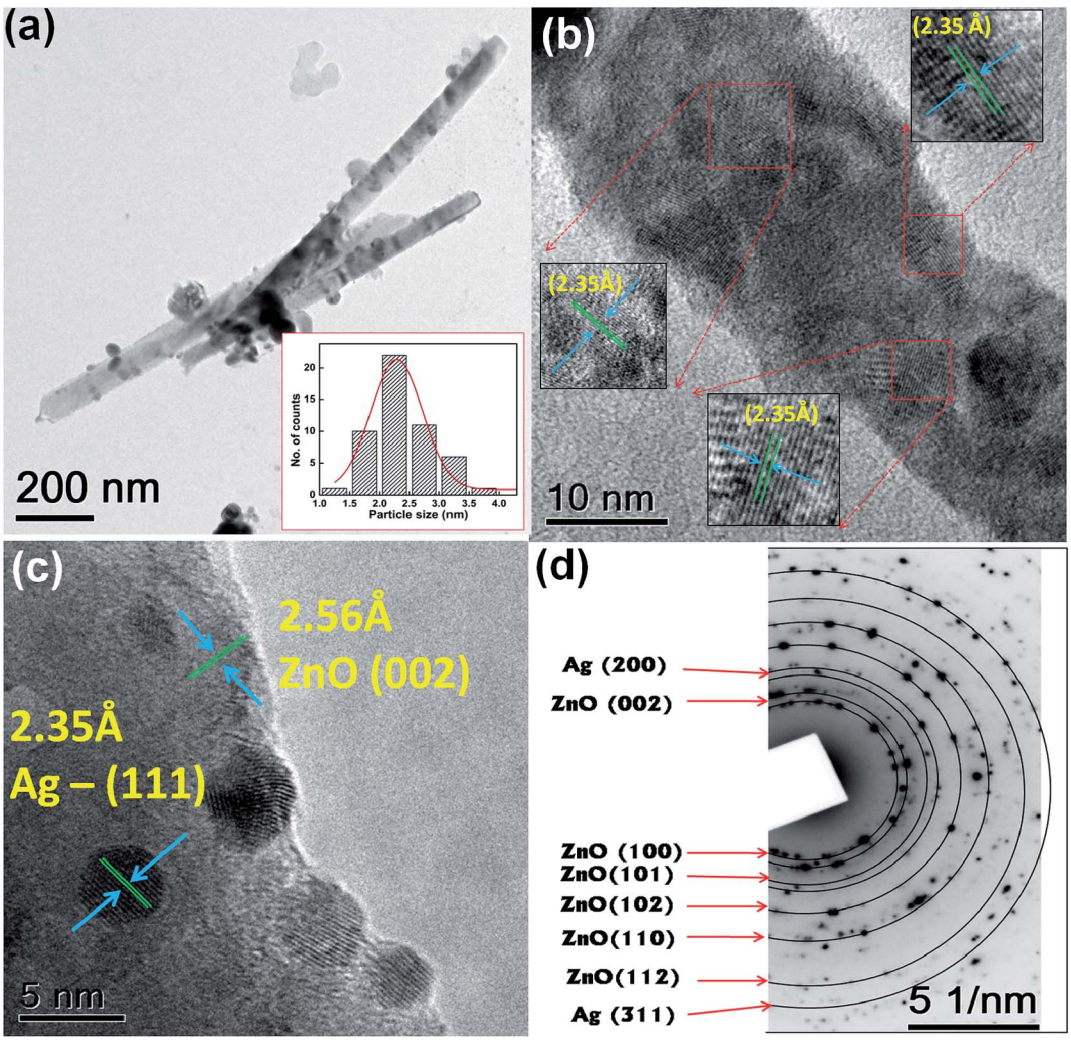

Fig. 3 (a) Representative TEM images of hybrid ZnO@Ag core–shell nanorods, high resolution TEM images showing (b) the Ag nanoclusters decorated over ZnO nanorods, (c) surface doped Ag nanoclusters and (d) SAED pattern analysis of hybrid ZnO@Ag core–shell nanorods.

images, ZnO nanorods of uniform length and width were obtained using the hydrothermal synthesis. Similarly, TEM analysis (Fig. 4b) divulges the well-defined boundaries of the nanorods. Selected area diffraction (SAD) studies reveals that the nanorods were grown from (100), (110) and (112) planes, and this matches well with the XRD studies (S2) of hexagonal wurtzite structured ZnO (JCPDS PDF no. 36-1451).

TEM analysis was carried out to infer about the structure and morphology of the hybrid ZnO@Ag core–shell nanorods. As evident from Fig. 3, the HRTEM image clearly shows the uniform distribution of Ag nanoclusters on the surface of the ZnO nanorods and confirms the formation of the hybrid nanostructures with core–shell hetero-junctions. Ag nanoclusters anchored onto the ZnO nanorods show an average particle size of ~2.5 nm (inset, Fig. 3a), and no aggregation was observed during the binding process, providing an effective synthetic process. The HRTEM image analysis (Fig. 3b and c) shows the notable interface structures with continuity of lattice fringes between the Ag nanoparticles and ZnO nanorods, which confirms the chemical bonding between the two particles. For ZnO nanorods, the adjacent lattice fringes space was calculated as 0.256 nm, which matches with the *d* spacing of the (002) plane of hexagonal structure, and hence confirms the single crystalline structure of ZnO nanorods with a preferred growth direction of [001] *c* axis.[34–37] Whereas, for Ag nanoclusters, the distance between adjacent lattice fringes was calculated as 0.235 nm, close to the *d*-spacing value of the (111) plane of fcc Ag. These values confirm that the [110] direction (*c* axis) is the preferred growth direction of the Ag nanoclusters, which matches with the XRD data. It is further confirmed by the HR-TEM analysis (Fig. 3c), showing the zone axis of fcc Ag along the [110] zone. The growth of Ag nanoclusters onto the ZnO nanorods occurs due to the lattice mismatch of Ag and ZnO.[35] Similarly, the SAED pattern (Fig. 3d) shows prominent ring patterns corresponding to ZnO and Ag. These mixed diffraction patterns confirm the presence of an Ag nucleus on the interfacial ZnO nanorods. This confirms the structure of ZnO@Ag core–shell nanorods during the seed mediated process using APTMS, which act as an active site for the growth of nanoclusters. The free amino group of APTMS can easily form a complex with Ag(I) creating active sites for silver cluster growth, which can also enhance the anchorage of Ag nanoclusters.[38] The resulting Ag(I)–amino-silanols complexes were reduced by TEA to form ZnO@Ag core–shell nanorods (Fig. 1).

XPS analysis was performed to corroborate the elemental and chemical states to elucidate the structure of the hybrid ZnO@Ag core–shell nanorods, and its corresponding spectra are depicted in Fig. 5. The binding energies observed in the XPS spectra are calibrated using C 1s (284.8 eV). All peaks in the Fig. 5a are ascribed to Zn, Ag, O and C elements, and no other peaks are observed, confirming that the sample composes of three elements, which match with the XRD and HR-TEM results. The carbon peak is likely to originate from the chamber contamination in the XPS equipment. Fig. 5b–d displays the high resolution spectrum of the Zn, Ag and O species, respectively. The peaks appearing in Fig. 5b are symmetric and centered at 1021.25 and 1044.65 eV, which are

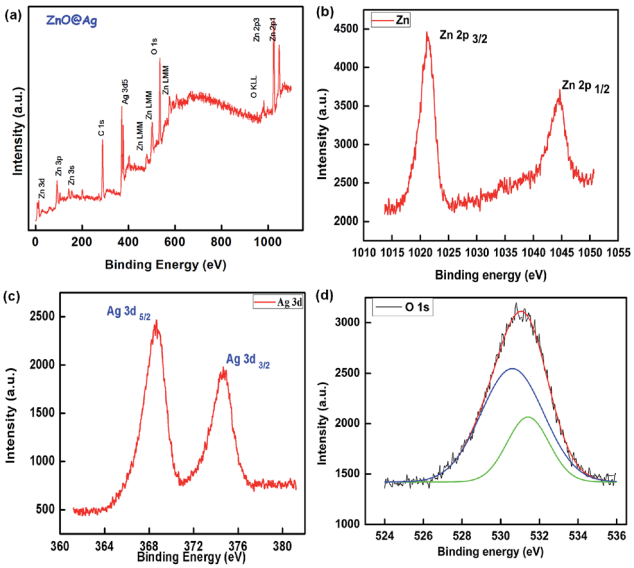

Fig. 5 XPS spectrum of the hybrid ZnO@Ag core–shell nanorods (a) survey peak full spectrum (b) Zn 2p spectrum (c) Ag 3d spectrum and (d) fitted O 1s spectrum.

attributed to Zn $2p_{3/2}$ and Zn $2p_{1/2}$, respectively. Because of the strong spin–orbital coupling, the Zn 2p peak splits into Zn $2p_{3/2}$ and Zn $2p_{1/2}$. The origin of the splitting is due to the charge transfer process between Zn^{2+} and O^{2-}, caused by vacancies.[39] This confirms the Zn presence in the Zn^{2+} state on the sample surface. From Fig. 5c, we can find that the binding energies for Ag $3d_{5/2}$ and Ag $3d_{3/2}$ matches with standard peaks for Ag (Ag $3d_{5/2}$ (368.2 eV) and Ag $3d_{3/2}$ (374.2 eV))[40] with an appreciable shift of 0.3 eV. This phenomenal shift is attributed to the interaction of the ZnO nanorods with Ag. Furthermore, differences in the work functions of Ag (4.26 eV) and ZnO (5.3 eV) enable the electron transfer from ZnO to Ag through the interfacial junctions during seed mediated growth.[33] The higher electronegative value of Ag compared to Zn initiates the electron transfer process from Zn to Ag, thus to confirm the chemical bonding between them. During the growth of Ag nanoclusters over the ZnO nanorods, fine-tuning of the Fermi level occurs.[19] Table S2 (see ESI†) summarizes the binding energy values for Zn 2p, Ag 3d and Os1, and its corresponding fwhm values.[41] It is noticed that small appreciable shifts in the binding energy values with the normal fwhm values of the elements reveal the presence of elements in their high defective states. In Fig. 5d, the O 1s profile asymmetric nature is observed with peaks positioned at 530.60 and 531.4 eV. This corresponds to the lattice oxygen of ZnO and oxygen related defects of Zn^{2+}. Further, the formation of hybrid ZnO@Ag core–shell nanorods were spectroscopically confirmed using FT-IR spectroscopy (see ESI, Fig. S4†), and thermal stability of the material was monitored using thermo-gravimetric analysis (see ESI, Fig. S5†).

Photocatalytic studies

The evaluation of photocatalytic activity was initially carried out for ZnO nanorods and hybrid ZnO@Ag core–shell nanorods

using rhodamine 6G (R6G) as the standard dye and, further evaluation was performed for two industrial textile dyes, namely, Congo red and Amido black 10B by both UV irradiation (λ = 360 nm) and solar irradiation (AM = 1.5 G). The photocatalytic activity of the material was studied by monitoring the degradation of standard R6G dye in an aqueous medium. Optical spectra obtained for the R6G dye during the photocatalytic degradation process (UV and solar irradiation) as a function of time are shown in Fig. 6 and S6 (see ESI†) for the ZnO@Ag and ZnO nanorods, respectively. The quantitative photocatalytic process could be monitored by studying the relative concentration changes in R6G dye during photocatalysis and by monitoring the characteristic absorbance of R6G at 525 nm. The photocatalytic degradation pattern observed by hybrid ZnO@Ag core–shell nanorods (Fig. 6a and b) for UV-irradiation and solar irradiation was found to pursue a similar pathway. The hybrid ZnO@Ag core–shell nanorods showed considerably faster degradation with 28 minutes photolysis time for complete degradation, whereas for ZnO nanorods, only partial decomposition was observed during this period as shown in Fig. 7. By plotting $\ln(C/C_o)$ as a function of time, the rate constant, k was obtained (see ESI, Fig. S7†).[42] The rate constant for R6G without the photocatalyst was found to be

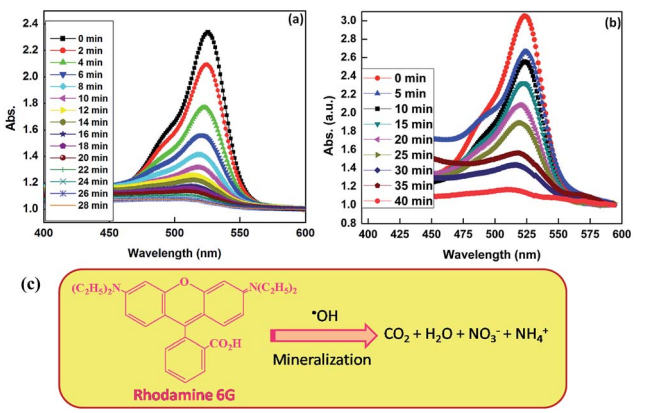

Fig. 6 Optical absorbance spectra monitoring the photocatalytic degradation process of R6G dye using ZnO@Ag core–shell nanorods (a) UV-irradiation, (b) solar-irradiation and (c) oxidative degradation pathway of R6G by ZnO@Ag core–shell nanorods.

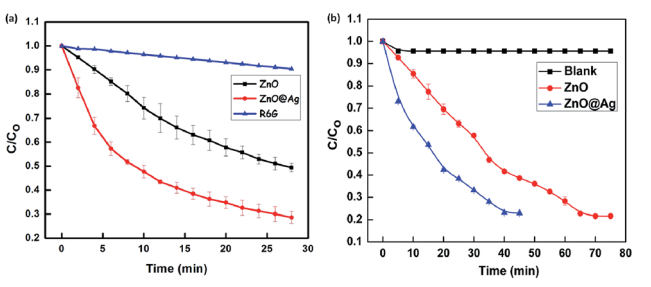

Fig. 7 Change in R6G concentration (C) relative to the initial concentration (C_o) during the photocatalytic degradation using ZnO, ZnO@Ag and blank as a function of time under (a) UV-irradiation and (b) solar-irradiation.

negligible under UV irradiation (4.3×10^{-4} min^{-1}) compared to ZnO and hybrid ZnO@Ag core–shell nanorods (vide Table S3†). It was observed that the hybrid ZnO@Ag nanorods exhibited higher photocatalytic activity as compared to the ZnO nanorods, since the Ag nanoclusters on the hybrid ZnO@Ag core–shell facilitate the interfacial charge transfer process, thus utilizing the CB electrons and acting as a reservoir for the free electrons.[32] Here, it is evident that the photocatalytic activity increases significantly for the hybrid ZnO@Ag core–shell nanorods as compared to the bare ZnO nanorods, which proves the positive role of the Ag nanoclusters in the photodegradation process. The photolysis time for 50% degradation of R6G dye using ZnO was 9 minutes, whereas for hybrid ZnO@Ag, photolysis time was decreased to 4 minutes. This enhanced photodegradation effect, observed by the hybrid materials compared to the ZnO nanorods alone, is endorsed due to the synergetic effect and charge transfer kinetic process carried out by the addition of Ag nanoclusters on the surface of the ZnO nanorods.[34] Moreover, the higher crystalline nature with a smaller size of Ag nanoclusters of hybrid ZnO@Ag core–shell nanorods plays an important role in the enhanced photocatalytic effect. From the photocatalysis results, it was observed that the photodegradation of R6G occurs through an oxidative pathway by photogenerated holes, leading to an irreversible permanent mineralization process.[43,44] The major end products after oxidative degradation of R6G are CO_2, H_2O, NO_3^- and NH_4^+, as shown in Fig. 6c.

In general, the photocatalytic process of hybrid ZnO@Ag based materials is a complex process and can be explained in detail using the band structure. The surface anchoring of noble metals on the surface of metal-oxides influence the interfacial charge transfer processes as depicted in Fig. 8. As the Fermi energy level of ZnO is higher than that of Ag, it will direct the migration of e^- from ZnO to the conduction band of Ag in order to achieve Fermi energy level equilibrium (E_f) (Fig. 8a). The irradiation of ZnO@Ag core–shell nanorods with energy equal to or higher (UV and solar irradiation) than the band gap energy

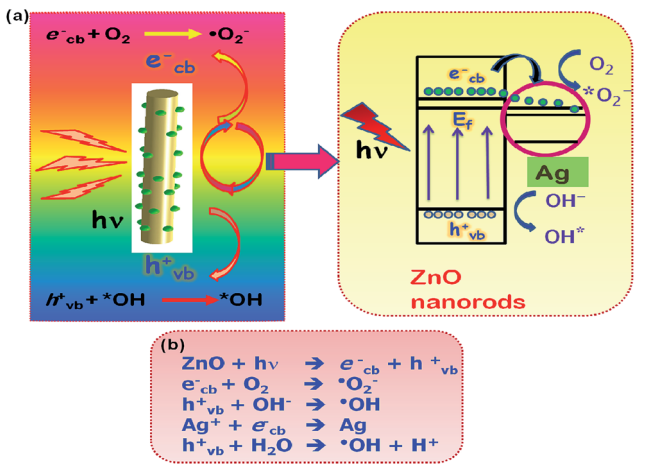

Fig. 8 (a) Mechanism of photocatalysis by hybrid ZnO@Ag core–shell nanorods, where Ag acts as a sink for photogenerated electrons and (b) corresponding electron transfer processes during photocatalysis.

results in the promotion of an electron (e^-) from the valance band (VB) to the conduction band (CB), leaving a hole (h_{vb}^+) in the valence band. The e_{cb}^- (photoelectrons) can be transferred from ZnO to Ag driven by the potential energy. Ag clusters, acting as an electron sink, thereby reduce the recombination of photoinduced electrons and holes but also prolong the lifetime of photogenerated pairs and moves them towards the surface of the particles. When moved towards the surface, electrons (e_{cb}^-) will be scavenged by the adsorbed oxygen molecule (O^2) and result in the formation of a superoxide anion radical ($^{\bullet}O_2^-$); whereas, holes (h_{vb}^+) generated at valence band will react with the surface bound hydroxyl groups (OH^-) and water molecules to form hydroxyl and hydroperoxyl radicals, respectively ($^{\bullet}OH$ and $^{\bullet}HO_2$), as shown in Fig. 8b.

In order to achieve enhanced photocatalysis, uniform surface anchoring of Ag nanoclusters is desirable, due to the active role of Ag and ZnO nanorods in the dye degradation process though an electron transfer process. Hence, an optimal loading of Ag nanoclusters is required. A drastic increase in the concentration of Ag nanoclusters on the ZnO nanorod surface induces the aggregation of Ag clusters into larger particles, which in turn decreases photocatalysis, as confirmed from XRD studies. In the hybrid ZnO@Ag core–shell nanorods, the Fermi level of Ag is lower than the ZnO nanorods (upon UV or solar irradiation), and hence the photo-excited electrons can be transferred from ZnO nanorods to Ag nanoclusters by the above driven potential energy due to the plasmonic effect.[45,46] Ag nanoclusters acts as an electron sink, since they generally reduce the recombination process of photoinduced e^- and h^+. It also increases the lifetime of the generated e^- and h^+ pairs. The electron transfer process will take place, until the overall Fermi level of hybrid ZnO@Ag nanorods is shifted to negative potential and equilibrates with the ZnO nanorods.[46] After attaining the equilibrium state, Ag nanoclusters discharge the captured

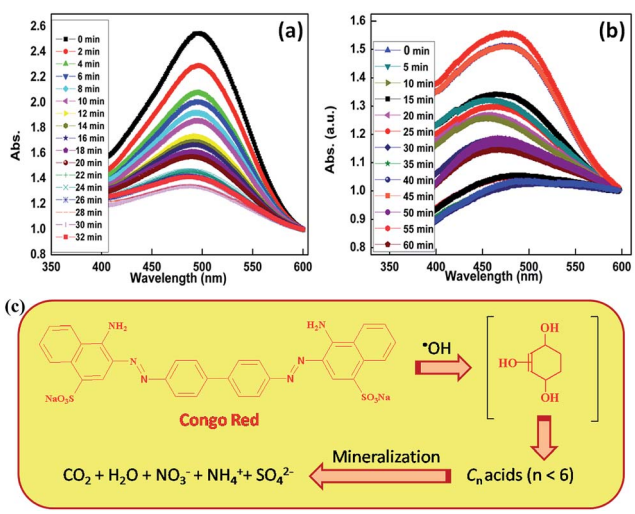

Fig. 9 Optical absorbance spectra monitoring the photocatalytic degradation process of Congo red using ZnO@Ag core–shell nanorods under (a) UV-irradiation, (b) solar-irradiation and (c) oxidative degradation pathway of Congo red by ZnO@Ag core–shell nanorods.

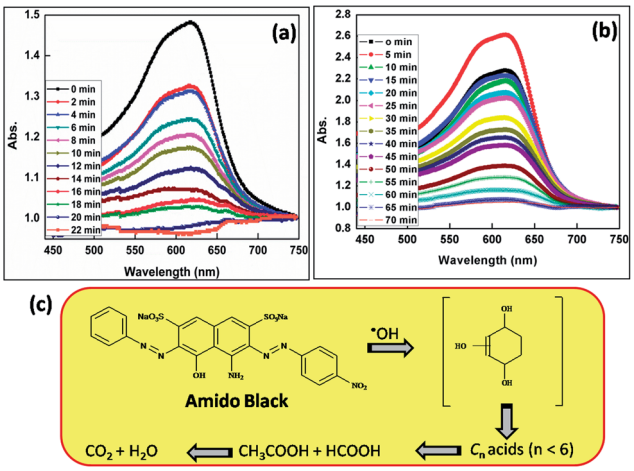

Fig. 10 Optical absorbance spectra monitoring the photocatalytic degradation process of Amido black 10B using ZnO@Ag core–shell nanorods (a) under UV-irradiation, (b) under solar-irradiation and (c) oxidative degradation pathway of Amido black 10B.

e^- into the solution, which in-turn reacts with the dissolved oxygen to form the superoxide and hydroxyl radicals. These highly reactive species ($^{\bullet}OH$, $^{\bullet}O_2^-$) will degrade the dye molecule into simpler molecules. Dye regeneration process is not possible in this system, as no back electron transfer process have been observed between the excited dye radical (R6G dye^+) and e^- (ZnO). This regeneration process was suppressed by Ag nanoclusters, which act as a sink for the CB free electrons (e_{cb}^-), and thus generate more VB holes (h_{vb}^+), which in turn promoted an enhanced photocatalytic process. Thus, Ag nanoclusters loaded onto the surface of ZnO nanorods facilitates the interfacial charge transfer process by utilizing the CB electrons, proving the significance of Ag in the photocatalytic process. The effect of varied pH conditions on the activity of ZnO@Ag hybrid core–shell nanorods was also monitored, which showed a varied % of degradation. Materials responded both in acidic and alkaline medium, and the maximum % of degradation was observed in the alkaline medium (see ESI, Fig. S8†). Similarly, the photocatalytic degradation of R6G dye was carried out using the hybrid ZnO@Ag core–shell nanorods under dark conditions (ESI, Fig. S9†). No major changes were observed for the

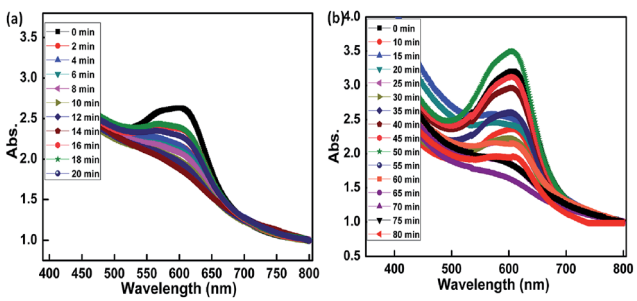

Fig. 11 Optical absorbance spectra monitoring the photocatalytic degradation process of the textile effluent using ZnO@Ag core–shell nanorods under (a) UV-irradiation and (b) solar-irradiation.

Table 1 Comparison of the %degradation efficiency and rate constant of R6G dye with industrial dyes and textile effluent, by ZnO nanorods and hybrid ZnO@Ag core–shell nanorods

	Degradation efficiency R6G dye		Degradation efficiency Congo red		Degradation efficiency Amido black 10B		Degradation efficiency textile effluent	
Sample	UV (%)	Solar (%)	UV (%)	Solar (%)	UV (%)	Solar (%)	UV (%)	Solar (%)
Blank	0.01	0.01	0.01	0.01	0.01	0.01	0.01	0.01
ZnO-NR	67	58	65	61	60	66	68	64
ZnO@Ag	98	89	97	87	97	90	92	94

characteristic peak monitored at 525 nm for 30 minutes, clearly emphasising that the degradation phenomenon was a photo-dependent process.

In order to investigate the efficiency of the ZnO@Ag core–shell nanorods in industrial textile dye degradation, commercial dyes widely used in dyeing industries, such as Congo red and Amido-black 10B were selected, and their photo-degradation studies were performed under both UV irradiation and solar irradiation. Similar experimental conditions applied for standard R6G were also adopted for these commercial dyes. Fig. 9a and b shows the degradation profiles of Congo red dye under UV and solar irradiation conditions. An oxidative pathway (Fig. 9c), followed by Congo red dye, was due to the photo generated holes, accordingly leading to the mineralization process and resulting in the production of CO_2, H_2O, NO_3^-, NH_4^+ and SO_4^{2-}.[47] From Fig. S10 (see ESI†), it can be understood that the catalytic activity increases noticeably for ZnO@Ag core–shell nanorods than ZnO nanorods, proving the effect of Ag nanoclusters. It is observed that the time corresponding to 50% dye degradation is 12 minutes for the hybrid ZnO@Ag nanorods when compared to ZnO nanorods, which is 22 min for UV irradiated samples; whereas, for solar irradiated samples, a similar pattern was observed with a faster degradation rate for the hybrid ZnO@Ag core–shell nanorods than ZnO nanorods (See Fig. S11, ESI†), indicating the positive role of Ag plasmonic effect in both UV irradiated and solar irradiated samples.

A similar degradation pattern was observed for Amido black 10B dye, and a higher catalytic activity was observed for hybrid ZnO@Ag nanorods compared to the ZnO nanorods. Fig. 10a and b depict the optical absorbance spectra showing the dye degradation profile of Amido black 10B under UV irradiated and solar irradiated conditions, respectively. The degradation process observed by Amido black 10B dye suggests that the photogenerated holes were responsible for the oxidative pathway followed by an irreversible permanent mineralisation process.[48] Similarly, Fig. S12† shows the optical absorbance spectra for ZnO nanorods under UV and solar irradiated conditions. As evident from Fig. S13a (see ESI†), the time taken for 50% degradation of dye for ZnO nanorods was 26 minutes, but for hybrid ZnO@Ag core–shell nanorods, it was observed to be 12 minutes under UV irradiation, owing to the enhanced photocatalytic effect due to its hybrid core–shell nanostructure. Similarly, for solar irradiated samples, the degradation pattern followed by hybrid ZnO@Ag was faster as compared to the ZnO nanorods (vide Fig. S13b, ESI†), indicating the positive role of the plasmonic effect of Ag nanoclusters. Degradation studies were carried out for textile effluent samples collected from a textile industry located in Thirupur, India, whose pH was neutralized to 7 from 9. A higher catalytic activity was observed for hybrid ZnO@Ag nanorods, compared to the ZnO nanorods, for the degradation of the effluent. Fig. 11 and S14† depict the optical absorbance spectra showing the dye degradation profile for the textile effluent using ZnO@Ag core–shell nanorods and ZnO nanorods, respectively. The time taken for 50% degradation of the effluent for ZnO nanorods (see ESI, Fig. S15†) was 24 minutes, but for the hybrid ZnO@Ag core–shell nanorods, it was observed to be 8 minutes, owing to the enhanced photocatalytic effect due to the hybrid core–shell nanostructure for UV irradiated samples.

For all the dyes used in this investigation, the hybrid ZnO@Ag core–shell nanorods showed an enhanced photocatalytic activity with a rate constant (k), compared to ZnO nanorods (see ESI, Table S3†). The phenomenal increase in the rate constant value of the hybrid nanomaterials can be attributed to the plasmonic enhancement due to the presence of Ag nanoclusters. Moreover, nanoclusters with a very small size and large surface area provide more active sites for charge carriers to react with surface absorbed molecules to form radical species. The degradation efficiency of the hybrid ZnO@Ag core–shell nanorods showed a maximum degradation, compared to ZnO (vide Table 1), for both UV irradiated and solar irradiated samples, indicating the enhanced effect of Ag nanoclusters due to the plasmonic effect. This proves that the hybrid ZnO@Ag core–shell nanorods can be used as an effective photocatalytic material and can be an alternative for conventional TiO_2 based systems during textile effluent treatment processes.

Conclusions

To summarize, a two-step, facile process based on a combined hydrothermal and seed mediated growth was used to develop hybrid ZnO@Ag core–shell nanorods, constituting Ag nanoclusters on the surface of ZnO nanorods. As a seed mediated growth method, the controlled deposition of Ag nanoclusters onto the ZnO surface has been achieved, as evident from the XRD studies. The core–shell nanorods constituents of ZnO@Ag were morphologically and structurally confirmed by SEM, TEM and XPS studies. The presence of a characteristic SPR band in the UV-visible spectra of the hybrid core–shell nanorods along with the excitonic peak of ZnO nanorods clearly indicates the

formation of hybrid nanostructured materials. It was observed that [111] facets Ag were grown over ZnO nanorods ([001] facets) in a morphologically controlled manner. UV emission observed in the PL spectra of the hybrid core–shell nanorods was found to be dramatically quenched, indicating the suppression of the electron–hole recombination process. The hybrid ZnO@Ag core–shell nanorods were found to exhibit excellent photocatalytic properties towards the degradation of R6G, Congo red and Amino black 10B dyes owing to the plasmonic effects of the Ag nanoclusters on the ZnO nanorods surface under UV and solar irradiations. The ZnO@Ag core–shell nanorods also showed good dye degradation properties for real time industrial textile effluent samples. The photocatalytic process was found to be enhanced for the hybrid ZnO@Ag core–shell nanorods, compared to the ZnO nanorods, due to an interfacial charge transfer process. The plasmonic Ag nanoclusters located on the surface of ZnO nanorods act as electron sinks, inducing the formation of holes in the valance band and electrons in the conduction band, respectively, which in-turn enhances the photocatalytic efficiency. The results prove that hybrid ZnO@Ag core–shell nanorods are promising materials with excellent photocatalyic properties owing to the plasmonic effect and can be effectively used for industrial textile dye degradation processes during effluent treatments.

Acknowledgements

The authors wish to acknowledge the facilities and support provided by the management, PSG Sons and Charities, Coimbatore and Materials Science Group, IGCAR, Kalpakkam. The authors wish to acknowledge Dr R. Kalpana, Department of English, PSG College of Technology, Coimbatore, India for proof reading and language correction.

References

1 I. K. Konstantinou and T. A. Albanis, *Appl. Catal., B*, 2004, **49**, 1–14.
2 S. Ameen, M. S. Akhtar, Y. S. Kim and H. S. Shin, *Appl. Catal., B*, 2011, **103**, 136–142.
3 V. Meshko, L. Markovska, M. Mincheva and A. E. Rodrigues, *Water Res.*, 2001, **35**, 3357–3366.
4 S. P. Sampatrao and M. S. Vijay, *Environ. Sci. Technol.*, 1988, **22**, 1160–1165.
5 T. M. Alan, V. Alex and F. Samuel, *Environ. Sci. Technol.*, 1989, **23**, 403–406.
6 L. T. Tracy and T. Y. John, *Chem. Rev.*, 2006, **106**, 4428–4453.
7 K. Vinodgopal, D. E. Wynkoop and P. V. Kamat, *CHEMTECH*, 1996, **4**, 18.
8 P. V. Kamat, *Chem. Rev.*, 1993, **93**, 267–300.
9 Y. Zheng, C. Chen, Y. Zhan, X. Lin, Q. Zheng, K. Wei, J. Zhu and Y. Zhu, *Inorg. Chem.*, 2007, **46**(16), 6675–6682.
10 D. Pingfan, S. Lixin, X. Jie and C. Houbao, *J. Mater. Sci.*, 2013, **48**, 8386–8392.
11 Z. Xiang, T. Velmurugan, S. G. Mhaisalkarb and R. Seeram, *Nanoscale*, 2012, **4**, 1707–1716.
12 N. Serpone, D. Lawless and R. Khairutdinov, *J. Phys. Chem.*, 1995, **99**, 16646.
13 U. Nayane, L. Myeongsoon, K. Junhyung and L. Dongil, *ACS Appl. Mater. Interfaces*, 2011, **3**, 4531–4538.
14 M. A. Mahmoud, W. Qian and M. A. EI-Sayed, *Nano Lett.*, 2011, **11**, 3285–3289.
15 D. B. Ingram and S. Linic, *J. Am. Chem. Soc.*, 2011, **133**, 5202–5205.
16 C. H. Chen, S. J. Chang, S. P. Chang, M. J. Li, I. C. Chen, T. J. Hsueh and C. L. Hsu, *Appl. Phys. Lett.*, 2009, **95**, 223101.
17 C. H. Ye, Y. Bando, G. Z. Shen and D. Golberg, *J. Phys. Chem. B*, 2006, **110**, 15146–15151.
18 L. Rui, W. Ping, W. Xuefei, Y. Huogen and Y. Jiaguo, *J. Phys. Chem. C*, 2012, **116**, 17721–17728.
19 M. R. Jones, K. D. Osberg, R. J. Macfarlane, M. R. Langille and C. Mirkin, *Chem. Rev.*, 2011, **111**, 3736–3827.
20 L. Myeongsoon, A. Piyadarsha, K. Junhyung and L. Dongil, *J. Phys. Chem. C*, 2010, **114**, 18366–18371.
21 Y. H. Zheng, C. Q. Chen, Y. Y. Zhan, X. Y. Lin, Q. Zheng, K. M. Wei and J. F. Zhu, *J. Phys. Chem. C*, 2008, **112**, 10773–10777.
22 N. Yong-hong, W. Xian-Wen, H. Jian-ming and Y. Yin, *Mater. Sci. Eng., B*, 2005, **121**, 42–47.
23 L. Peng, W. Zhe, W. Tong, P. Qing and L. Yadong, *J. Am. Chem. Soc.*, 2011, **133**, 5660–5663.
24 Y. C. Lu, Y. H. Lin, D. J. Wang, L. L. Wang, T. F. Xie and T. F. Jiang, *J. Phys. D: Appl. Phys.*, 2011, **44**, 315502.
25 T. Linnert, P. Mulvaney, A. Henglein and H. WeUer, *J. Am. Chem. Soc.*, 1990, **112**, 4657–4664.
26 P. B. Sarawade, S. M. Kim, K. D. Kim and H. T. Kim, *J. Ind. Eng. Chem.*, 2014, **20**, 1830–1833.
27 Z. Y. Huang, G. Mills and B. Hajek, *J. Phys. Chem.*, 1993, **97**, 11542.
28 M. J. Hostetler, J. E. Wingate, C. J. Zhong, J. E. Harris, R. W. Vachet, M. R. Clark, J. D. Londono, S. J. Green, J. J. Stokes, G. D. Wignall, G. L. Glish, M. D. Porter, N. D. Evans and W. R. Murray, *Langmuir*, 1998, **14**, 17–30.
29 T. J. Sun, J. S. Qiu and C. H. Liang, *J. Phys. Chem. C*, 2008, **112**(3), 715–721.
30 S. A. Studenikin, N. Golego and M. Cocivera, *J. Appl. Phys.*, 1998, **84**, 2287.
31 K. Vanheusden, C. H. Seager, W. L. Warren, D. R. Tallant and J. A. Voigt, *Appl. Phys. Lett.*, 1996, **68**, 403–406.
32 L. Jaeil, S. S. Hyeong, L. Myeongsoon, K. S. Jae and L. Dongil, *J. Phys. Chem. Lett.*, 2011, **2**, 2840–2845.
33 V. Subramanian, E. E. Wolf and P. V. Kamat, *J. Phys. Chem. B*, 2003, **107**, 7479–7485.
34 H. R. Liu, G. X. Shao, J. F. Zhao, Z. X. Zhang, Y. Zhang, J. Liang, X. G. Liu, H. S. Jia and B. S. Xu, *J. Phys. Chem. C*, 2012, **116**, 16182–16190.
35 H. Xiangyun, D. Jiangnan, Y. Chenhui, W. Zhihao, C. Changqing and G. Yihua, *Appl. Surf. Sci.*, 2010, **256**, 4682–4686.
36 *CRC Handbook of Chemistry and Physics*, ed. W. M. Haynes, CRC/Taylor & Francis, BocaRaton, FL, 95th edn, 2014.
37 Z. Rui, G. Y. Peng, W. Ning and G. Lin, *Solid State Sci.*, 2009, **11**, 865–869.

38 W. Sun, G. Chen and L. Zheng, *Scr. Mater.*, 2008, **59**, 1031–1034.
39 Y. Y. Tay, S. Li, C. Q. Sun and P. Chen, *Appl. Phys. Lett.*, 2006, **88**, 173118–1731111.
40 J. F. Moudler, W. F. Stickle, P. E. Sobol and K. D. Bomben, *Handbook of X-ray Photoelectron Spectroscopy*, Perkin-Elmer, Eden Prairie, MN, 1992.
41 K. S. Ranjan, K. Ganguly, T. Mishra, M. Mishra, R. S. Ningthoujam, S. K. Roy and L. C. Pathak, *J. Colloid Interface Sci.*, 2012, **366**, 8–15.
42 J. Zeng, M. Xin, K. W. Li, H. Wang, H. Yan and W. Zhang, *J. Phys. Chem. C*, 2008, **112**, 4159–4167.
43 I. K. Konstantinou and T. A. Albanis, *Appl. Catal., B*, 2004, **49**, 1–14.
44 T. S. Natarajan, M. Thomas, K. Natarajan, H. C. Bajaj and R. J. Tayade, *Chem. Eng. J.*, 2011, **169**, 126–134.
45 M. Jakob, H. Levanon and P. V. Kamat, *Nano Lett.*, 2003, **3**, 353.
46 Z. Yuanhui, Z. Lirong, Z. Yingying, L. Xingyi, L. Z. Qi and W. Kemei, *Inorg. Chem.*, 2007, **46**(17), 6980–7986.
47 T. S. Natarajan, K. Natarajan, H. C. Bajaj and R. J. Tayade, *Ind. Eng. Chem. Res.*, 2011, **50**, 7753–7762.
48 A. V. Salker and S. D. Gokakakar, *Int. J. Phys. Sci.*, 2005, **4**(6), 377–384.